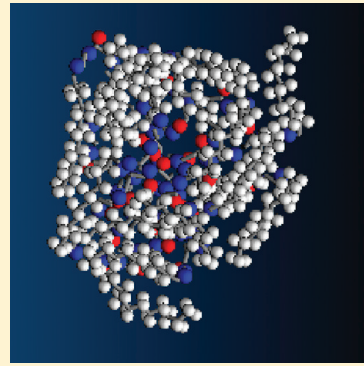


Stability of Amphiphilic Dendrimers at the Water/Air Interface

Selina Nawaz and Paola Carbone*

School of Chemical Engineering and Analytical Science, The University of Manchester, Oxford Road, M13 9PL, United Kingdom

ABSTRACT: By means of atomistic molecular dynamics simulations, we investigate the structure and stability of alkyl-modified polyamido-amide (PAMAM) dendrimers at the air/water interface as a function of the number and the relative position of the modified end groups. We find that the PAMAM dendrimer with all terminal groups functionalized is more stable at the interface than the Janus dendrimer where only half the amine groups are modified. This result is explained in terms of softness of the dendrimer molecule which adapts its conformation to maximize the favorable amide–water contacts segregating the alkyl chains and increasing the structural order of the “hydrophilic core”. We interpret the stability of the molecule at the interface also in terms of particle wettability and energy components. We verify that the atomistic model follows the prediction of the thermodynamic analytical theory adopting an oblate or prolate shape and orientating its longest axis parallel to the normal to the interface. These results indicate that monolayers of fully functionalized molecules could be as stable as (or more stable than) those self-assembled from proper Janus molecules.



■ INTRODUCTION

In recent years, amphiphilic dendrimers have shown to be promising building blocks for a large range of interfacial materials. In fact, tailor-made dendrimers show interesting self-assembly properties when strong dispersive, polar, or hydrogen bonding intermolecular forces are present.^{1,2} In particular, alkyl-modified hydrophilic dendrimers such as poly(amino amide) (PAMAM) or poly(propylene imine) form a Langmuir–Blodgett monolayer at the surface or interface that, due to the large number of functionalities present in their hydrophilic core, can show high stability. Indeed, amphiphilic dendrimers can bind at the interface more efficiently than classical surfactants, and because of dendrimers' unique topology, their monolayers find a wide number of applications such as surface-based sensors or surface nanopatterning.^{3,4} Recently, the physical characterization of the Langmuir–Blodgett monolayer formed at the air–water interface by amphiphilic PAMAMs fully functionalized with long aliphatic chains has been the subject of intensive experimental investigations.^{5–7} Amphiphilic dendrimers can also self-assemble in aqueous media forming micelles whose stability is a function of the shape of the functionalized dendrimer molecules.² Moreover, through a specific synthetic route, dendrimers can also be modified targeting specifically one side of the molecule. This type of synthetic procedure allows the preparation of amphiphilic “Janus” dendrimers, where the hydrophobic chains are attached only to part of the end monomers, breaking the symmetry of the macromolecule (see Figure 1).^{8–11} In this case, the bipolar nature of the molecules allows the formation in water of a large variety of self-assembled structures that can be exploited for several applications such as encapsulation or delivery of drugs. The Janus dendrimers can be seen as an example of a Janus nanoparticle whose properties and applications have been foreseen as very innovative due to the dual nature of the particle that, especially at interfaces, can bind different substrates.¹²

Computer simulations can help in predicting the behavior of amphiphilic molecules both in bulk and at the interface. Using simplified models, it is possible for example to calculate the free energy profile of ideal nanoparticles at the interface, predicting their stability as a function of shape, orientation, and distance from the interface.^{13–15} Similar simplified models have also been used to study the strength of the interaction between a spherical model Janus nanoparticle at an ideal fluid interface studying how the particle–interface stability is controlled by changing the difference in affinities between the two particle regions and their relative sizes.¹⁶ Moreover, in the particular case of dendrimers, using simplified models it has been predicted that amphiphilic dendrimers interacting via a purely repulsive Gaussian potential crystallize into a cubic lattice with density-independent lattice constants.¹⁷ However, while simplified models are very useful to gain properties common to a large family of molecules,¹⁸ atomistic models are needed when one wants to investigate the specific chemical interactions responsible, for example, for molecular aggregation¹⁹ or intramolecular rearrangements.^{19,20} Despite this, besides the simplified models that idealize the nanoparticle as a compact impenetrable sphere, simulations of nanoparticles at the interface that use an atomistic description of molecules are almost absent in the literature. The only work we are aware of is that of Tay and Bresme²¹ who reported the results of atomistic molecular dynamics simulations performed on an alkylthiol passivated gold nanoparticle absorbed at the air–water interface predicting the contact angle, particle shape, and orientational order of the water molecules.

Received: June 22, 2011

Revised: August 19, 2011

Published: September 14, 2011

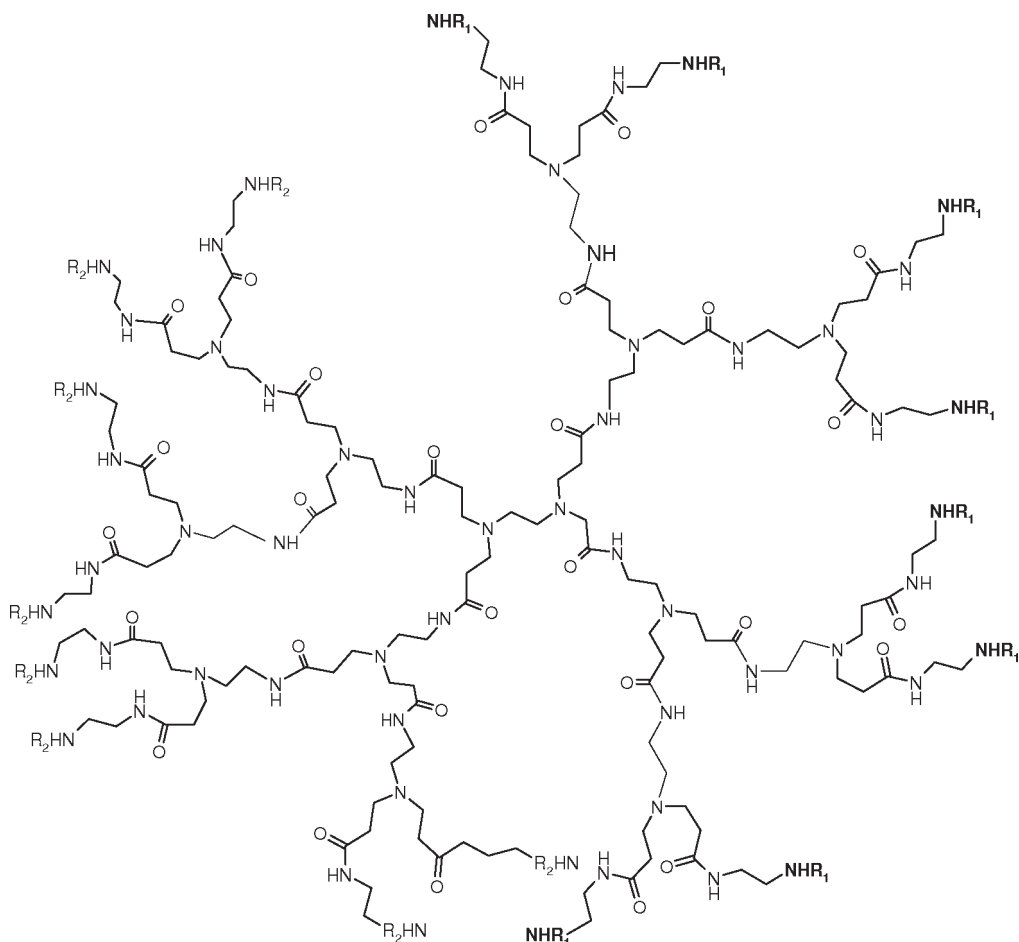


Figure 1. Poly(amino amide) dendrimer of second generation. In the fully functionalized dendrime, $R_1 = R_2 = C_{10}H_{23}$. In the Janus dendrimer, $R_1 = C_{10}H_{23}$, while $R_2 = H$. In the unmodified dendrimer, $R_1 = R_2 = H$.

This paper aims at covering partially this gap clarifying and predicting the stability of a single amphiphilic PAMAM dendrimer (fully modified and Janus dendrimer) at the air/water interface by means of atomistic molecular dynamics simulations. The structural properties of the molecule at the interface, the molecular interactions responsible for the diffusion of the dendrimer toward the interface, and the interface stability are investigated also in terms of wetting properties and particle shape and compared with the thermodynamic model predictions. The ultimate goal of this investigation is to help in the design of new dendrimeric molecular structures with target properties rationalizing the different non-bonded interactions responsible for the molecular aggregations.

■ COMPUTATIONAL DETAILS

One PAMAM dendrimer molecule of second generation (16 terminal groups) is functionalized with either 16 (pure amphiphilic dendrimer) or 8 (Janus dendrimer) *n*-decane chains. In the Janus dendrimer, the eight *n*-decane chains are attached in a symmetric fashion to have the aliphatic chains attached to the terminal NH_2 groups belonging to the same side of the amine dendrimer core (see Figure 1). The functionalized dendrimer models are obtained adding 16 (fully functionalized) or 8 (Janus) *n*-decane chains to the NH_2 primary amine terminal groups of well-equilibrated unfunctionalized PAMAM dendrimer models.¹⁹ The force field parameters and the steps followed to equilibrate the

unfunctionalized models are reported in ref 19 and here only briefly described. The force field employed during the simulations is the OPLS-AA force field developed specifically for primary amines²² and amides.²³ The OPLS-AA force field has shown to be a reliable force field for polyamides characterized by different topologies being able to reproduce their thermodynamic (density, glass transition temperature, thermal expansion coefficient)^{19,24} and structural (radius of gyration, hydrogen bonds)^{25,26} experimental properties. The unfunctionalized PAMAM models are initially pre-equilibrated in vacuum using a Monte Carlo algorithm and then put randomly oriented in a simulation box of large size. The bulk system is then subjected to a series of energy minimization and soft core MD runs until the proper density is reached. From this well equilibrated PAMAM dendrimer bulk, one molecule is extracted and functionalized adding either 16 (fully functionalized dendrimer) or 8 (Janus dendrimer) *n*-decane chains. The molecule is then subjected to energy minimization to initially equilibrate the structure. Four different systems are set up and simulated. The dendrimer model (both fully functionalized and Janus) is put either inside the water phase or at the air/water interface. The interface is built, simulating a cubic water box with 4000 molecules of SPC water²⁷ for 1 ns in an NPT (constant temperature and pressure) ensemble until the correct density of liquid water at room temperature and atmospheric pressure is reached. The simulation box is then increased in the Z-direction, and the dendrimer is immersed into the water phase (or placed at the interface),

Table 1. List of the Simulated Systems

model	position of the dendrimer model	number of water molecules	simulation box size (nm)	simulations length
fully functionalized	inside the water phase	3798	5.0 × 5.0 × 15.0	25 ns
fully functionalized	at the air/water interface	3784	5.0 × 5.0 × 15.0	40 ns
Janus	inside the water phase	3886	5.0 × 5.0 × 15.0	25 ns
Janus	at the air/water interface	3882	5.0 × 5.0 × 15.0	40 ns

Table 2. Radius of Gyration (R_g), Eigenvalues (λ_i), and Aspect Ratios (α) of the Gyration Tensor with the Corresponding Standard Deviations^a

model	R_g (nm)	λ_1 (nm)	λ_2 (nm)	λ_3 (nm)	$\alpha_{12} = \lambda_1/\lambda_2$	$\alpha_{13} = \lambda_1/\lambda_3$
Janus	1.05 ± 0.02	0.77 ± 0.03	0.57 ± 0.03	0.41 ± 0.02	1.35 ± 0.07	1.88 ± 0.08
fully functionalized	1.18 ± 0.03	0.86 ± 0.03	0.66 ± 0.04	0.46 ± 0.03	1.30 ± 0.08	1.88 ± 0.09

^a The average is performed over the last 10 ns of the trajectory for two different starting configurations.

removing all the water molecules whose atoms overlap the dendrimer ones. The system is further minimized before starting the simulations. Two different starting configurations for each system are used. Table 1 summarizes the characteristics of the simulated systems. The simulations where the dendrimer molecule is placed into the water phase are carried out to investigate the time scale and the molecular mechanism responsible for the migration of the dendrimer toward the interface. For the equilibration and production runs, the very high-frequency bond stretching vibrations are removed using rigid constraints which allow us to use an integration time step of $\Delta t = 2$ fs. Long simulations (up to 40 ns) in NVT (constant temperature and volume) at 300 K are run with a thermostat coupling time of 0.1 ps and a cut off of 1.0 nm. The long-range electrostatic interactions are treated using the reaction field method using the dielectric constant of the water (72) for the continuum.²⁸ The simulations are carried out with the GROMACS package.^{29–32}

RESULTS

Structural Properties of the Dendrimer at the Interface. Analytical studies based on thermodynamic models predict that the stability of a generic nanoparticle at the interface depends upon a complicated interplay between particle shape, line tension, and particle orientation. In general, elongated (prolate) nanoparticles show a reduced stability compared with spherical and oblate ones, although for a small interval of aspect ratio α ($1 < \alpha < 1.904$), α being the ratio between the two semi axis, the prolate particles show to be stable. Moreover, an oblate particle whose symmetry axis is parallel to the normal vector of the interface shows the highest stability, while the prolate particles with the symmetry axis perpendicular to the vector normal to the interface have higher stability than those whose symmetry axis is parallel to it.¹³

Detailed atomistic simulations enable us to monitor the change in the 3D molecular shape by the calculation of the second moment of the atomic distribution (the gyration tensor) which is defined as³³

$$\mathbf{R}_{\alpha,\beta}^2 = \frac{1}{N} \sum_{i=1}^N (\mathbf{r}_\alpha^i - \mathbf{r}_\alpha^M)(\mathbf{r}_\beta^i - \mathbf{r}_\beta^M) \quad \alpha, \beta = x, y, z \quad (1)$$

where N is the number of atoms in the molecule; \mathbf{r}_α^i is the position of the i th atom; and \mathbf{r}_α^M is the position of the dendrimer's geometrical center. The eigenvalues of the gyration tensor (λ_1^2 , λ_2^2 , and λ_3^2)

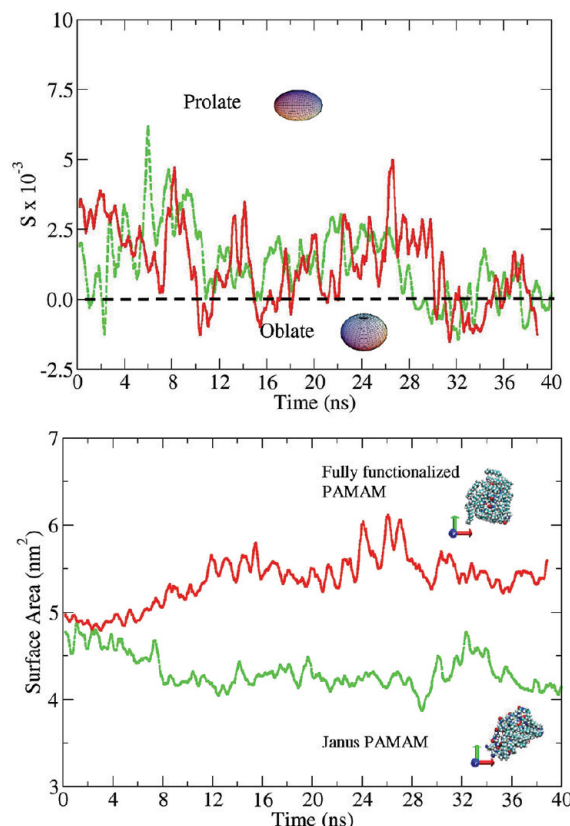


Figure 2. Degree of prolateness (S) and surface area (SA) for the fully functionalized (solid red line) and Janus (dashed green line) dendrimer at the interface. The results are shown for only one of the two simulation runs for each model. In the molecular structures (low panel): the oxygen, nitrogen, and carbon atoms are depicted in red, blue, and cyan, respectively. Water molecules are omitted for clarity. The vision of the molecule is from the top along the Z-axis in the vacuum phase.

represent the characteristic lengths of the equivalent ellipsoid with which the dendrimer is described. From the knowledge of the λ_i , it is possible to calculate the degree of prolateness that can be measured through the parameter S where $S = [(\lambda_1 - \bar{\lambda}) \cdot (\lambda_2 - \bar{\lambda}) \cdot (\lambda_3 - \bar{\lambda})] / \bar{\lambda}^3$ and $\bar{\lambda}$ is the mean eigenvalue of the gyration tensor.³⁴ For prolate rodlike shape $S = 2$ (being $\lambda_1 \neq 0$; $\lambda_2 = \lambda_3 = 0$), $S = -1/4$ for an oblate disk-like object (where $\lambda_1 = \lambda_2$; $\lambda_3 = 0$) and $S = 0$ for spherical

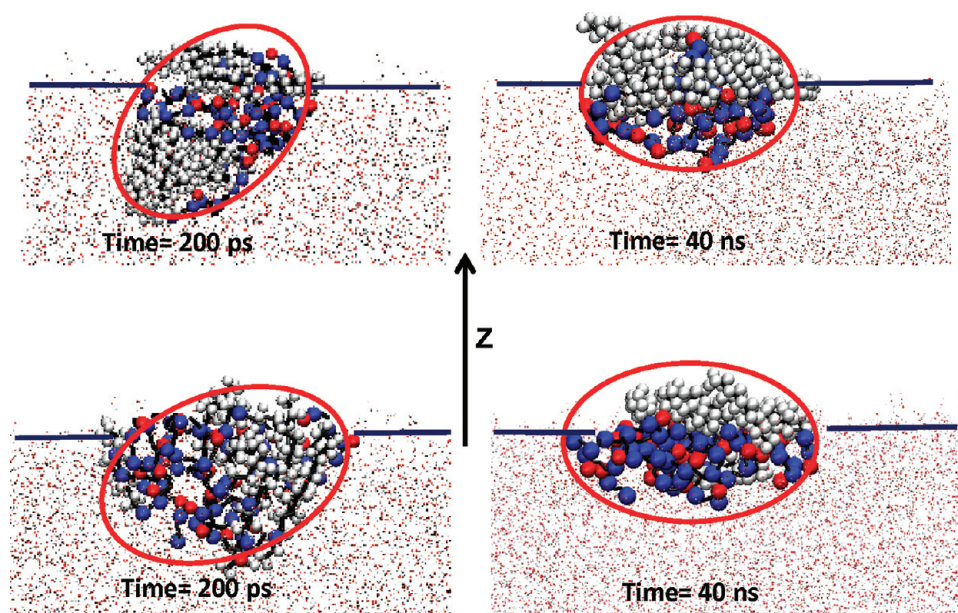


Figure 3. Snapshots of the fully modified (top panel) and Janus (lower panel) dendrimer at the interface at the beginning and end of the simulation. The ellipse is drawn to help to visualize the orientation of the molecule with respect to the Z-axis. For the molecular structure: the oxygen and nitrogen atoms are depicted in red and blue, respectively. The only hydrogen atoms bonded to the alkyl chains are pictured (white); the water molecules are pictured as points.

shape (where $\lambda_1 = \lambda_2 = \lambda_3$). In general $S > 0$ for prolate ellipsoid-like molecules, and $S < 0$ for the oblate ones. Table 2 reports the values for the gyration radius and the corresponding eigenvalues averaged over the last 20 ns of the two sets of simulations carried out for each system simulated, while Figure 2a shows how the value of S , calculated for the fully functionalized and Janus dendrimers placed at the interface, changes during simulation. From the plots in Figure 2a, we observe that the approximated 3D shape of both dendrimer models oscillates between the two most stable configurations predicted by the theory (oblate and prolate). Table 2 reports also the value of the aspect ratio α_{12} and α_{13} calculated using either the smallest eigenvalue (λ_3) or the middle one (λ_2). The aspect ratios are also in good agreement with the interval of stability predicted by the theory ($1 < \alpha < 1.904$). Unlike the surface area of a sphere, the surface area of a general ellipsoid cannot be expressed exactly by an elementary function; however, knowing the eigenvalues (λ_i) of the gyration tensor, it is possible to calculate its approximated surface area (SA) through the following formula

$$SA \approx 4\pi \left(\frac{\lambda_1^p \lambda_2^p + \lambda_1^p \lambda_3^p + \lambda_2^p \lambda_3^p}{3} \right)^{1/p} \quad (2)$$

where p is a constant. This approximation has the least relative error ($\pm 1.061\%$ in the worst case) when $p = 1.6075$.^{35,36} Figure 2b shows the SA calculated using eq 2 for the two models placed at the interface along with the top view of the fully functionalized and Janus dendrimer at the end of the simulation. It is interesting to notice that while for the fully modified PAMAM the rearrangement of the hydrophobic chains increases the total SA of the molecule, for the Janus model this rearrangement leads to a decrease of its SA. In fact, as we will show with more detail below, during the simulation, the fully functionalized dendrimer changes its global shape, adopting a conformation that enables a large part of the polar atoms of the hydrophilic dendrimer core to interact with the water, increasing in this way its interfacial area.

Although, due to the intrinsic flexibility of the molecular structure, both the Janus and the fully functionalized dendrimers modify their shape, their orientation at the interface agrees with the analytical predictions.¹⁵ The value of the angle between the Z-axis (perpendicular to the interface plane) and the eigenvector (Λ) corresponding to the highest eigenvalue of the gyration tensor oscillates in fact around 90° ($90^\circ \pm 20^\circ$ averaged over the last 20 ns of the simulations). This result can be inferred also from Figure 3 that depicts the structure of the models after 200 ps and at the end of the simulation. From the figure, it can be seen that the fully functionalized dendrimer initially rotates slightly at the interface and changes its relative orientation from perpendicular to the interface to parallel to it. The Janus dendrimer rotates as well from a tilted conformation to a parallel one. From the figure, it appears also clear that in both models the hydrophilic amide groups and the hydrophobic aliphatic chains tend to segregate within the molecule. We can quantify this segregation calculating the atomic mass density distribution across the simulation box (in the Z-direction). Figure 4 shows the change of the density distributions of the apolar atoms (carbon atoms of the alkyl chain) and polar atoms (defined as the nitrogen and oxygen of the amide groups) during the simulation. What appears clearly from the density profiles is that the fully modified dendrimer, when initially placed inside the water phase, cannot expose its hydrophilic part to the water molecules due to the presence of the aliphatic chains that form a hydrophobic layer around it. However, approaching the interface, the hydrocarbon chains unwrap, revealing the dual nature of the molecule. Figure 4a shows that, when the fully functionalized PAMAM dendrimer is inside the water phase, the polar and apolar atoms distribution is symmetric with respect to the Z-axis. However, when the dendrimer approaches the interface, this symmetry is broken, and the aliphatic chains extend toward the air while the hydrophilic part of the dendrimer is more exposed to water. On the contrary, the Janus dendrimer, due to the distribution of the alkyl chains within the molecule, shows a

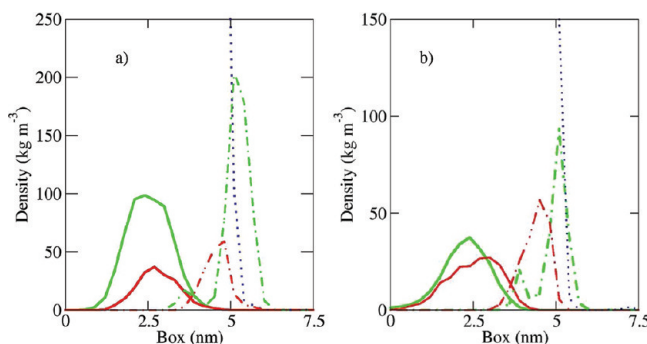


Figure 4. Mass density distribution calculated across the interface of the apolar atoms (i.e., carbon atoms of the aliphatic chain) (green line), polar atoms (i.e., nitrogen and oxygen atoms) (red line), and water molecules (dotted blue line) when inside the water phase (solid lines) and when at the interface (point-dashed lines). (a) The fully functionalized dendrimer. (b) The Janus dendrimer.

clear separation between the hydrophilic and hydrophobic parts even when it is immersed into the water phase. When the molecule reaches the interface, the separation becomes more evident; however, in contrast with what happens for the fully functionalized molecule, a large part of the aliphatic chains is either still in contact with the water or partially immersed in it (Figure 4b). The clustering of the aliphatic chains occurring in the fully modified PAMAM can be quantified calculating their interchain carbon–carbon radial distribution function (RDF). Figure 5a reports the RDFs calculated for the fully functionalized dendrimer at three different stages of the simulation. From the plots, it can be noticed that the segregation between the hydrophobic and hydrophilic blocks starts to occur when the dendrimer is still in the water phase. Indeed, within the first 8 ns, when the molecule is still immersed in the water, the first two peaks of the RDF become higher, indicating that the alkyl chains self-segregate within the molecule. Once the dendrimer has reached the interface (after ca. 10 ns), the segregation of the aliphatic chains continues especially at medium distance. To investigate how the self-organization of the aliphatic chains affects the structure of the polar region of the dendrimer, we calculate the RDF for the nitrogen atoms. To avoid taking into account contributions to the RDF coming from nitrogen atoms belonging to the same dendron (which do not reflect the reorganization of the molecule), we calculate the RDF only between the eight end-monomer tertiary amine nitrogen atoms (Figure 5b). The plots show that the segregation of the aliphatic chains within the molecule leads to a different rearrangement of the polar part of the molecule: after the first 8 ns, the first peak of the RDF is slightly shifted to lower distance, while the other peaks of the distribution lie more far apart. More remarkably, the RDFs show that the reorganization of the apolar block of the dendrimer induces a more ordered structure in the inner hydrophilic part of the dendrons that opens up, to allow the aliphatic chains to come together, and becomes more prone to the formation of hydrogen bonds with the water (see next section). Once the dendrimer has reached the interface, the RDF changes again, showing that the polar atoms pack more tightly, losing its long-range order. On the contrary, the Janus dendrimer does not show any remarkable changes in its RDFs, and this is reflected in the constant number of hydrogen bonds it forms with the water molecules (see next section). The calculation of the dihedral distributions along the aliphatic chains shows

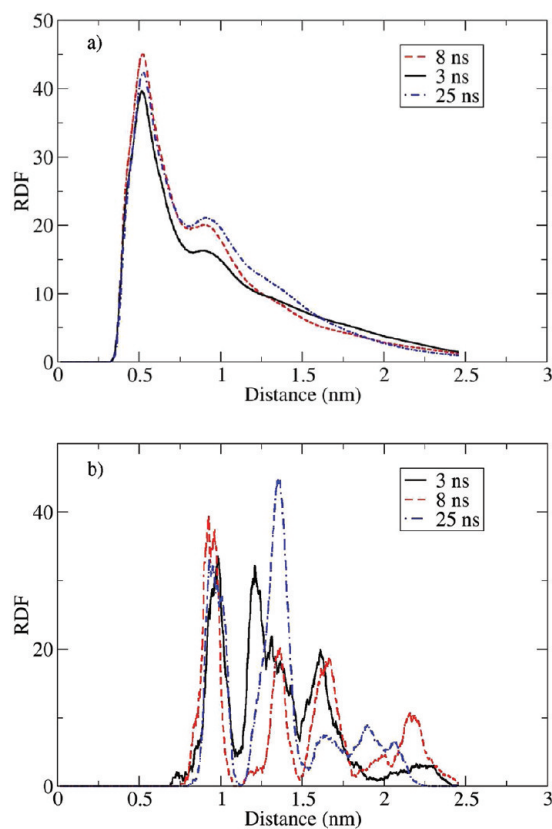


Figure 5. Interdendron radial distribution function (RDF) calculated for the carbon atoms belonging to the alkyl chains (a) and for the tertiary amine nitrogen atoms (b) of the fully functionalized dendrimer. The RDFs are calculated between 2–3 ns, 7–8 ns, and 24–25 ns.

that they are mainly in an extended conformation irrespective of the degree of functionalization of the end groups. The percentage of *trans* conformation changes from 78% (for the fully functionalized model) and 73% (in the Janus model) when the dendrimer is in the water phase to 90% (for the fully functionalized) and 80% (for the Janus dendrimer) once the dendrimer has reached the interface. Moreover, the chains are organized mainly parallel to the air–water interface (as can be inferred also from Figures 2 and 3). In fact, the average angle calculated between the vector connecting the first and the last carbon atom of each alkyl chain and the normal to the air–water interface (identified as the *z*-axis) is 104 ± 13 for the Janus dendrimer and 116 ± 15 for the fully functionalized ones.

Hydrogen Bonds and Particle Stability. In this section of the paper, we investigate whether the intradendrimer or dendrimer–water hydrogen bonds (HBs) affect the stability of the molecule at the interface and whether their number changes following the change in the global conformation of the dendrimer molecules. The HBs have been identified following the geometrical criteria reported in refs 19 and 37 that showed to be able to provide results in agreement with X-ray experimental data. To consider a donor (X_d)–acceptor (X_a) couple hydrogen-bonded, the distance between them has to be below 0.3 nm (d_{HB}) and the donor-hydrogen–acceptor ($X_d\text{H}\cdot X_a$) angle above 130° (ϑ_{HB}). These criteria are broad enough to include all possible HBs formed in the model and are consistent with the NMR findings.¹⁹ Figure 6a reports the number of HBs calculated from the simulation of the fully functionalized dendrimer when the molecule is initially

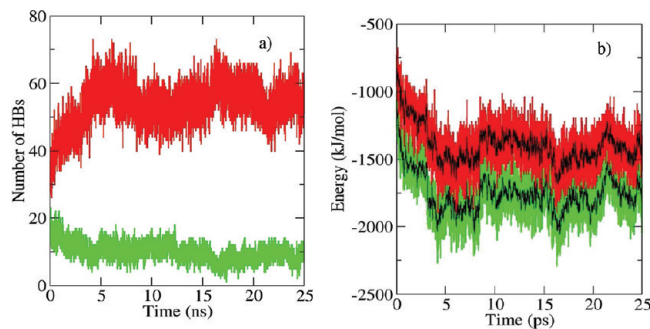


Figure 6. Fully functionalized PAMAM dendrimer: (a) number of dendrimer–dendrimer (green) and dendrimer–water (red) hydrogen bonds; (b) short-range Coulomb energy (calculated among atoms whose distance is less than or equal to 1.1 nm) (green) and HB energy (red). The black line shows the running average (averaged every 20 ps).

placed into the water phase. During the 25 ns simulation, the dendrimer moves toward the interface and approaches it after ca. 10 ns. Here it is important to notice that this time scale is typical for this particular simulation and that different starting configurations lead to slightly different time scales. For example, in our second simulation the dendrimer reaches the interface after ca. 15 ns. However, although the time required for the dendrimer to approach the interface can vary, the variation in the number of HBs with the time is the same in our two simulations: while the dendrimer migrates toward the interface, the number of dendrimer–water HBs constantly increases until reaching a plateau value around which it oscillates, while the number of intradendrimer HBs slightly decreases. The plateau value, reached in the case reported in Figure 6a after ca. 5 ns, is the same for the two simulations carried out on the fully functionalized dendrimer and corresponds to 57 ± 4 . It is clear from these results that initially the presence of the aliphatic chains wrapped around the hydrophilic dendrimer core prevents the formation of HBs between the amide groups of the dendrimer whose number, however, increases within the first ca. 5 ns of the simulation. These results are in agreement with what is observed from the RDFs reported in Figure 5a, which shows that approaching the interface the alkyl chains self-assemble, trying to minimize their contact with the water, while the hydrophilic “core” of the dendrimer opens up, allowing the formation of HBs with the water molecules. When the dendrimer is directly placed at the interface, the number of HBs (both intradendrimer and dendrimer–solvent) does not change during the entire simulation time (not shown), and their numbers (10 ± 3 and 58 ± 4 , respectively) are consistent with the plateau values that can be inferred from Figure 6a.

Monitoring the different components of the total internal energy of the system while the dendrimer approaches the interface, it can be noticed that the short-range (calculated among atoms whose distance is less than or equal to 1.1 nm) electrostatic energy calculated between the dendrimer and the water molecules shows the largest variation (500 kJ/mol ca.). The energy component initially constantly decreases (see Figure 6b) and then reaches a plateau. Interestingly, the number of dendrimer–water HBs and the short-range Coulomb energy change with the time in a similar fashion: an increase in the number of HBs corresponds to a decrease in the short-range Coulomb energy. To make this relation more clear, we can associate an energy value to the formation of each HB. Quantum chemical calculations have shown that an averaged value of -26 kJ/mol ³⁸ can be associated

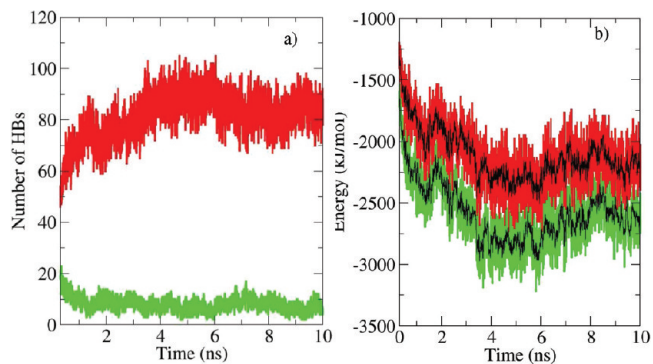


Figure 7. Unfunctionalized PAMAM dendrimer: (a) number of dendrimer–dendrimer (green) and dendrimer–water (red) hydrogen bonds; (b) short-range Coulomb energy (calculated among atoms whose distance is less than or equal to 1.1 nm) (green) and HB energy (red). The black line shows the running average (averaged every 20 ps).

to the formation of one HB between an amide group and a water molecule. We can then calculate the total energy due to the creation of the HBs multiplying the number of HBs reported in Figure 6a by -26 kJ/mol . Figure 6b reports the energy obtained in such a way and compares it with the change in the short-range Coulomb energy. The two energy profiles follow indeed the exact same pattern. To further analyze the effect of the HBs on the position of the dendrimer with respect to the interface, a new simulation with unmodified PAMAM dendrimer ($R_1 = R_2 = H$ in Figure 1) of second generation is set up. The simulation is carried out following the procedure described in the previous section. The dendrimer is placed at the air–water interface, and a NVT simulation ($T = 300 \text{ K}$) is run for 10 ns. After ca. 3 ns, the dendrimer has completely moved into the water phase. At this point, we also calculate the radius of gyration of the unfunctionalized dendrimer in the water phase to further verify our force field choice. The R_g obtained (0.92 ± 0.01) agrees well with previous computational and experimental studies.^{39–41} Also, in this case the major change in the internal energy of the system is due to the decrease of the dendrimer–water short-range Coulomb interactions during the first 3 ns of the simulation. Figure 7b shows the short-range (atomic distance less than or equal to 1.1 nm) Coulomb energy calculated among the dendrimer and the water molecules and the corresponding HB energy considering again that each HB corresponds to -26 kJ/mol . The two energy profiles perfectly match also in this case. These results show that the major contribution to the change (decrease) in the total internal energy of the system is due to the formation of the dendrimer–water HBs whose number increases when the alkyl chains self-assemble. They also show that the HBs drive the migration of the dendrimer toward the air–water interface and that the corresponding energy represents the major component of the short-range Coulomb interactions. Moreover, Figure 6b proves that the OPLS-AA force field^{22,23} is a reliable interatomic potential for polyamides being able to reproduce the correct energy for the amide–water HBs. Similar calculations are performed on the Janus dendrimer. In this case, the number of HBs (63 ± 5) does not change when the dendrimer travels toward the interface, showing that the aliphatic chains, being attached only to one side of the molecule, do not hinder the formation of HBs between the water and the amide groups whose number is slightly higher than that of the fully functionalized PAMAM. However, this also shows that the amide groups belonging to the

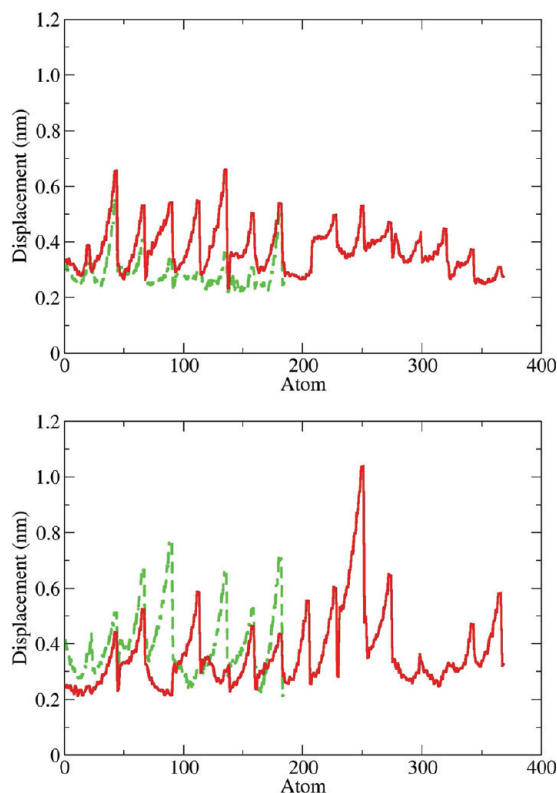


Figure 8. Root mean square fluctuation (RMSF) of the hydrogen atoms attached to the alkyl chains of the Janus (green dashed line) and fully functionalized (red solid line) dendrimer, when the dendrimer is in the water phase (top) and when it is at the interface (bottom).

arms functionalized with the *n*-decane are restrained in their conformation probably for steric reasons. To verify this hypothesis, we calculate the root mean squared fluctuation (RMSF) of the position of the hydrogen atoms attached to the alkyl chains around the averaged structure. Figure 8 shows that, at the beginning of the simulation (1.5–3.5 ns), the aliphatic chains attached to the Janus dendrimer are on average less mobile than those attached to the fully functionalized one; however, once the aliphatic chains have rearranged, their relative mobility is reversed, and the chains attached to the fully modified PAMAM become on average less mobile than those of the Janus molecule. This fact can be explained considering that in the water phase the aliphatic chains surrounding the amphiphilic “core” of the fully modified dendrimer try to avoid contact with the water molecules, while the amide groups of the core form HBs as soon as they are enough close to them. This metastable situation leads to frequent intramolecular conformational changes. Once the dendrimer is at the interface, the segregation of the apolar and polar parts of the molecule imparts a peculiar conformation to the dendrimer that tries to maximize the energetic favorable contacts. All the aliphatic chains tend to separate from the water interface and segregate as much as the topology of the molecule allows. This creates a very crowded environment around the aliphatic carbons (and so around the hydrogen covalently bonded to them) that hampers the motion of the atoms. In the case of the Janus dendrimer, on the contrary, the fact that the polar and apolar parts of the molecule are separated topologically makes energetically more stable the dendrimer into the water phase. In fact, in the water solution, the amide groups belonging

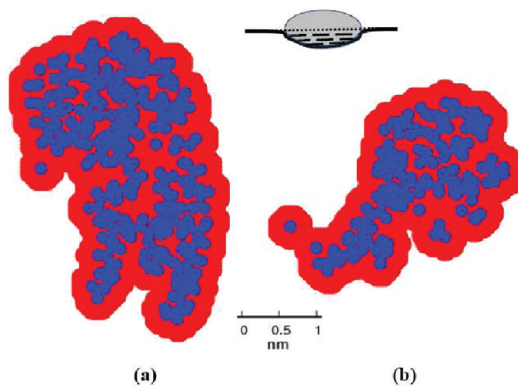


Figure 9. Area per dendrimer (red) at the interface calculated using the geometrical method as reported in the text for (a) the fully modified dendrimer and (b) the Janus dendrimer. The atom positions are shown in blue and correspond to the configuration after 10 ns of simulation. In the figure, the prolate nanoparticle at the interface is also schematically represented in 2D. The volume calculated in the text corresponds to the dashed area.

to the unfunctionalized dendrons form HBs with the water, while the others form intradendrimer HBs. Once the dendrimer reaches the interface, the aliphatic chains that extend out from the interface show a less restrained dynamics than that of the fully functionalized dendrimer. In fact, their number being half of the number of the fully functionalized dendrimer, they are less sterically constrained.

As described in the previous section, both amphiphilic dendrimers investigated here adopt at the interface either an oblate or a prolate shape with the highest eigenvector of the gyration tensor perpendicular to the Z-axis (see Figures 3 and 4). Moreover, we have showed that a large part of the alkyl chains of the fully functionalized dendrimer emerged from the water phase extending into the vacuum, while for the Janus molecule the apolar chains are largely submerged by the water molecule. We can further analyze the stability of dendrimers at the interface by looking at their wetting properties such as the contact area. In fact, particles with a large contact area show higher stability than those with a smaller one. From our simulations, we can calculate the area of the dendrimer at the water–air interface, slicing the dendrimer in the Z direction and taking only those atoms whose centers of mass lie at the interface (that corresponds to $z = 0$ nm). To calculate the area, a 2D grid is built around the portion of the molecule in contact with the interface (see Figure 9). The mesh of the grid is tuned until the resulting area converges. For the fully functionalized dendrimer, the area calculated in such a way and averaged over the last 2 ns of the simulation is $780 \pm 20 \text{ \AA}^2$. This result can be reasonably compared with the experimental limiting molecular area obtained for the PAMAM dendrimer of generation 3 (16 endgroups) but modified with lauroyl chloride ($\text{C}_{11}\text{H}_{23}\text{COCl}$), that is, $676 \pm 1 \text{ \AA}^2$. It is, in fact, expected the experimental value to be smaller than the simulated one as the data are extrapolated at zero surface pressure under maximum packing conditions. The same calculation using the last 2 ns of the simulation of the Janus dendrimer gives an area of $660 \pm 7 \text{ \AA}^2$. The fact that the Janus dendrimer shows a smaller area at the interface compared with the fully modified one agrees with the results obtained from the calculation of the surface area and degree of prolateness and may indicate that, surprisingly, the topologic dual nature of the Janus molecule does not increase its

stability at the interface. In fact, the flexible structure of the dendrimer and its symmetric topology allow the fully modified molecule to change its behavior depending on which environment it is placed in.

SUMMARY AND CONCLUSIONS

By means of atomistic molecular dynamics simulation, we have investigated the stability of the alkyl-modified polyamino amide dendrimer (PAMAM) at the air–water interface as a function of the number and relative position of the functionalized terminal amine groups. In particular, we have simulated two types of amphiphilic dendrimers: one where all the amine terminal groups are modified with *n*-decane and another where only half of the terminal groups (in a symmetric fashion) are functionalized (Janus particle). We used our simulations to test the most recent thermodynamic theories developed for nanoparticles at interfaces and to compare the relative stability of two macromolecules characterized by different topological structure.

We found that both our models follow the theoretical predictions in terms of particle orientation and particle shape. In fact, the dendrimers are oriented with their longest axis perpendicular to the normal of the interface line. Due to the topology of the molecule, its shape oscillates between the predicted two most stable shapes (oblate and prolate) with their aspect ratio α also in agreement with the theoretical value.

The dendrimer mass density distribution calculated across the interface showed that the Janus dendrimer is largely submerged by the water molecules, while the alkyl chains of the fully functionalized PAMAM stand out from the water phase and extend toward the vacuum.

We observed that in the case of the fully functionalized model the molecular interactions that govern the migration of the dendrimer toward the interface are the dendrimer–water hydrogen bonds (HBs). Similar simulations performed on the unmodified PAMAM dendrimer of the same generation showed that the dendrimer–water HBs are also responsible for the motion of the hydrophilic dendrimer from the air–water interface into the water phase.

We showed that when the amphiphilic dendrimer is into the water phase the long aliphatic chains are initially wrapped around the hydrophilic part of the dendrimer and hinder the formation of the intermolecular HBs. Within the first 10–15 ns, the alkyl chains unwrap and segregate, avoiding the contact with the water solvent, and the dendrimer migrates toward the interface.

We noticed that the clustering of the alkyl chains starts when the dendrimer is still submerged by the water and leads to a more ordered structure for the hydrophilic dendrimer “core” which opens up and forms HBs with the water solvent. On the contrary, in the case of the Janus dendrimer, the number of HBs when the molecule is at the interface does not differ from their number when the molecule is into the water phase, showing that the asymmetric topology of the dendrimer does not require any major changes to minimize its energy.

Calculating the interfacial contact area between the dendrimer and the water, we observed that the fully modified PAMAM molecule shows a higher contact area than the Janus one, confirming that the former is characterized by a more oblate 3D shape than the latter.

These results indicate that, due to the topology of the molecule and the flexibility of its dendrons, the fully functionalized dendrimer shows better stability at the interface than the Janus one. This latter result may indicate that monolayers of fully modified

dendrimers are characterized by the same or higher stability than the monolayer of the Janus dendrimer, confirming the extraordinary versatility of dendrimeric molecules and the necessity of atomistic molecular modeling to gain a complete picture of their behavior.

AUTHOR INFORMATION

Corresponding Author

*E-mail: paola.carbone@manchester.ac.uk.

ACKNOWLEDGMENT

The authors thank Aline Miller for useful discussions.

REFERENCES

- (1) Tully, D. C.; Frechet, J. M. J. *Chem. Commun.* **2001**, 1229–1239.
- (2) Frechet, J. M. J. *Proc. Natl. Acad. Sci. U.S.A.* **2002**, 99, 4782–4787.
- (3) Pericet-Camara, R.; Cahill, B. P.; Papastavrou, G.; Borkovec, M. *Chem. Commun.* **2007**, 266–268.
- (4) Tokuhisa, H.; Crooks, R. M. *Langmuir* **1997**, 13, 5608–5612.
- (5) Sui, G.; Mabrouki, M.; Ma, Y.; Micic, M.; Leblanc, R. M. *J. Colloid Interface Sci.* **2002**, 250, 364–370.
- (6) Zhang, T.; Dvornic, P. R.; Kaganove, S. N. *Langmuir* **2007**, 23, 10589–10597.
- (7) Chooi, K. W.; Gray, A. I.; Tetley, L.; Fan, Y. L.; Uchegbu, I. F. *Langmuir* **2010**, 26, 2301–2316.
- (8) Esfand, R.; Tomalia, D. A. *Drug Discovery Today* **2001**, 6, 427–436.
- (9) Lee, C. C.; MacKay, J. A.; Frechet, J. M. J.; Szoka, F. C. *Nat. Biotechnol.* **2005**, 23, 1517–1526.
- (10) Rosen, B. M.; Wilson, C. J.; Wilson, D. A.; Peterca, M.; Imam, M. R.; Percec, V. *Chem. Rev.* **2009**, 109, 6275–6540.
- (11) Percec, V.; Wilson, D. A.; Leowanawat, P.; Wilson, C. J.; Hughes, A. D.; Kaucher, M. S.; Hammer, D. A.; Levine, D. H.; Kim, A. J.; Bates, F. S.; et al. *Science* **2010**, 328, 1009–1014.
- (12) Walther, A.; Muller, A. H. E. *Soft Matter* **2008**, 4, 663–668.
- (13) Faraudo, J.; Bresme, F. *J. Chem. Phys.* **2003**, 118, 6518–6528.
- (14) Cheung, D. L.; Bon, S. A. F. *Phys. Rev. Lett.* **2009**, 102, 066103–066107.
- (15) Bresme, F.; Oettel, M. *J. Phys.: Condens. Matter* **2007**, 19, 413101–413134.
- (16) Cheung, D. L.; Bon, S. A. F. *Soft Matter* **2009**, 5, 3969–3976.
- (17) Mladek, B. M.; Kahl, G.; Likos, C. N. *Phys. Rev. Lett.* **2008**, 100, 028301–028305.
- (18) Carbone, P.; Lue, L. *Macromolecules* **2010**, 43, 9191–9197.
- (19) Carbone, P.; Müller-Plathe, F. *Soft Matter* **2009**, 5, 2638–2647.
- (20) Carbone, P.; Calabretta, A.; Di Stefano, M.; Negri, F.; Müllen, K. *J. Phys. Chem. A* **2006**, 110, 2214–2224.
- (21) Tay, K. A.; Bresme, F. *J. Am. Chem. Soc.* **2006**, 128, 14166–14175.
- (22) Rizzo, R. C.; Jorgensen, W. L. *J. Am. Chem. Soc.* **1999**, 121, 4827–4836.
- (23) Jorgensen, W. L.; Maxwell, D. S.; TiradoRives, J. *J. Am. Chem. Soc.* **1996**, 118, 11225–11236.
- (24) Goudeau, S.; Charlot, M.; Müller-Plathe, F. *J. Phys. Chem. B* **2004**, 108, 18779–18788.
- (25) Roberts, B. P.; Krippner, G. Y.; Scanlon, M. J.; Chalmers, D. K. *Macromolecules* **2009**, 42, 2784–2794.
- (26) Karimi-Varzaneh, H. A.; Carbone, P.; Müller-Plathe, F. *Macromolecules* **2008**, 41, 7211–7218.
- (27) Berendsen, H. J. C.; Grigera, J. R.; Straatsma, T. P. *J. Phys. Chem.* **1987**, 91, 6269–6271.
- (28) Tironi, I. G.; Sperb, R.; Smith, P. E.; van Gunsteren, W. F. *J. Chem. Phys.* **1995**, 102, 5451–5459.
- (29) Berendsen, H. J. C.; Postma, J. P. M.; van Gunsteren, W. F.; Di Nola, A.; Haak, J. R. *J. Chem. Phys.* **1984**, 81, 3684–3690.

- (30) Berendsen, H. J. C.; van der Spoel, D.; van Drunen, R. *Comput. Phys. Commun.* **1995**, 43–56.
- (31) Lindahl, E.; Hess, B.; van der Spoel, D. *J. Mol. Model.* **2001**, 7, 306–317.
- (32) Van der Spoel, D.; Lindahl, E.; Hess, B.; Groenhof, G.; Mark, A. E.; Berendsen, H. J. C. *J. Comput. Chem.* **2005**, 26, 1701–1718.
- (33) Theodorou, D. N.; Suter, U. W. *Macromolecules* **1985**, 18, 1206–14.
- (34) Blavatska, V.; Janke, W. *J. Chem. Phys.* **2010**, 133, 184903–184910.
- (35) Klamkin, M. S. *Am. Math. Mon.* **1971**, 78, 280–283.
- (36) Klamkin, M. S. *Am. Math. Mon.* **1976**, 83, 478.
- (37) Karimi-Varzaneh, H. A.; Carbone, P.; Muller-Plathe, F. *Macromolecules* **2008**, 41, 7211–7218.
- (38) Mitchell, J. B. O.; Price, S. L. *Chem. Phys. Lett.* **1991**, 180, 517–523.
- (39) Maiti, P. K.; Cagin, T.; Wang, G. F.; Goddard, W. A. *Macromolecules* **2004**, 37, 6236–6254.
- (40) Maiti, P. K.; Li, Y. Y.; Cagin, T.; Goddard, W. A. *J. Chem. Phys.* **2009**, 130, 10.
- (41) Rathgeber, S.; Monkenbusch, M.; Kreitschmann, M.; Urban, V.; Brulet, A. *J. Chem. Phys.* **2002**, 117, 4047–4062.